PHYSICAL REVIEW B **85**, 121203(R) (2012)

Magneto-optical analysis of the effective *g* tensor and electron spin decoherence in the multivalley conduction band of bulk germanium

C. Hautmann* and M. Betz

Experimentelle Physik 2, Technische Universität Dortmund, 44227 Dortmund, Germany

(Received 7 February 2012; published 29 March 2012)

We present a comprehensive study of electron spin decoherence in bulk germanium. As a first cornerstone, the effective *g* tensor of *L*-valley electrons in germanium is deduced from time-domain magneto-optical experiments. The decay of the ensemble spin polarization is then found to be closely related to intervalley scattering. In particular, the angular and temperature dependences of the experiment are well described in a model including Elliott-Yafet-type spin-flip processes as well as dephasing due to scattering between valleys exhibiting different effective *g* factors.

DOI: 10.1103/PhysRevB.85.121203 PACS number(s): 78.47.J−, 75.78.Jp, 78.20.Ls

The idea of exploiting the spin degree of freedom for devices brought about huge efforts to explore mechanisms of spin injection and decoherence in semiconductors. In particular, optical orientation offers efficient photon-to-spin conversion and is widely available in many compound semiconductors and their nanostructures.[1] Much less is known about spin generation and/or detection involving indirect optical transitions in the elementary semiconductors silicon and germanium (Ge), although indirect evidence of optical orientation of conduction-band electrons historically was first established in silicon.[2] Partially polarized luminescence for phonon-assisted transitions subsequent to electrical spin injection[3,4] or optical pumping[5] in silicon has been investigated experimentally and theoretically.[6] In Ge, electrical detection of electron spins oriented via direct transitions was reported.[7] Loren *et al*. examined carrier spin dynamics in Ge in an all-optical approach.[8] Their room-temperature experiments revealed subpicosecond hole spin relaxation. Our own magneto-optical measurements at low temperatures showed that circularly polarized light injects comparably long-lived partially spin-polarized electrons and holes in Ge via both direct and indirect optical transitions.[9] This study has been focused mainly on the optical orientation process, a detailed analysis of hole spin coherence, and the demonstration of remarkably robust electron spin coherence. However, the influence of the multivalley conduction-band structure of Ge remained unexplored. The anisotropic electron dispersion typical of *L*-valleys reduces the symmetry of the effective Landé tensor $\mathbf{g}^*$ (Refs. 10 and 11) compared to the isotropic situation in direct semiconductors where electrons are restricted to the Γ-valley. Consequently, an additional dephasing mechanism arises when intervalley scattering effectively changes the precession frequency. Those previously unaddressed questions are the subject of the present magneto-optical study of bulk Ge. In particular, we evaluate the Larmor precession of photoinduced electron spins for various in-plane magnetic-field orientations and crystallographic orientations to deduce $\mathbf{g}^*$. We then analyze electron spin decoherence as a function of temperature, doping concentration, and the crystallographic orientation. The observed dependences are explained by a model of spin decoherence in the multivalley conduction band.

I. EXPERIMENTAL METHOD AND SAMPLES

The experiment relies on the well known concept of time-resolved Faraday rotation (FR) in Voigt geometry. A 250 kHz optical parametric amplifier delivers ∼60 fs pulses tunable around 1500 nm. The samples are kept in a cryostat between 10 and 200 K and are exposed to in-plane magnetic fields $\vec{B}$ of up to $B = 2.1$ T. FR of the linearly polarized (degenerate) probe pulses is detected with a polarization bridge taking advantage of lock-in detection referenced to a 1.5 kHz modulation of the excitation.

The Ge samples are commercial optical grade *n*-type wafers. Room-temperature resistivities ρ, doping concentrations n_d, and thicknesses d are given in Table I. Data for samples A1 and A2 are provided by the manufacturer. The crystallographic orientation of sample B is determined by x-ray analysis, while resistivity and Hall measurements reveal carrier concentration and polarity.

FR transients are taken after excitation with circularly polarized pulses of a central wavelength of ∼1500 nm so that the photon energies $\hbar\omega = (0.82 \pm 0.02)$ eV are between the indirect $E_G = 0.72$ eV (0.68 eV) and the direct band gap $E_{\Gamma 1} = 0.89$ eV (0.84 eV) at 10 K (200 K). Consequently, the vast majority of interband transitions is indirect. Typical values for the photogenerated carrier density vary in the range of a few times 10^{16} cm^{-3} depending on lattice temperature and optical depth within the sample. The trends discussed below, however, do not depend strongly on the exact choice of this excitation density. To remove a slowly varying background from the transients, the presented data are extracted by subtracting FR signals for $\sigma+$ and $\sigma-$ polarized excitation.

II. RESULTS ON THE g* TENSOR

As a useful starting point, we discuss FR transients taken for different orientations α of the in-plane magnetic field $\vec{B}$. Data are taken at $T = 10$ K in $B = 2.1$ T. Figure 1(a) depicts FR transients for three different values of α obtained in the ⟨100⟩-oriented sample A1. They are characterized by pronounced Larmor precessions and an additional beating for certain orientations. Fast Fourier transformation (FFT) extracts the contributing Larmor frequency components $(\omega_L)_i$. As shown

TABLE I. Ge samples parameters. Samples A1 and A2: Umicore Electro-Optic Materials. Sample B: Edmund Optics.

Sample	Surface	ρ (Ω cm)	n_d (cm^{-3}) (dopant)	d (mm)
A1	$\langle 100\rangle$	66 ± 3	$(2.2 \pm 0.1) \times 10^{13}$ (Sb)	0.55
A2	$\langle 100\rangle$	0.045 ± 0.005	$(6 \pm 1) \times 10^{16}$ (Sb)	0.35
B	$\langle 111\rangle$	20 ± 1	$(6 \pm 2) \times 10^{13}$ (?)	1.5

in Fig. 1(b), they can be converted into effective g factors $g_i = \hbar(\omega_L)_i/(\mu_B B)$. Most strikingly, the peak positions in the FFT amplitude shift pronouncedly with the magnetic-field orientation. In addition, it is possible to find orientations where only one effective g factor contributes to the signal. This angular dependence arises from the anisotropic electron dispersion for L-valley electrons in Ge. Specifically, $\mathbf{g}^*$ is composed of two components g_l and g_t, and the effective g factor for electrons in one specific valley reads

$$g^2 = g_t^2 \sin^2\theta + g_l^2 \cos^2\theta, \tag{1}$$

where θ denotes the angle between $\vec{B}$ and the principal axis of the iso-energy ellipsoid.[12] In general, the four conduction-band minima at the L-valleys imply up to four different and angular-dependent Larmor frequencies. This situation is simplified for a highly symmetric $\langle 100\rangle$-oriented sample. As is illustrated in Fig. 2(b), the four equivalent L-valleys break down into only one or two classes of geometrical arrangements. For this surface orientation, the θ_i in Eq. (1) are

$$\cos(\theta_1) = \frac{2}{\sqrt{6}}\cos(\alpha), \quad \cos(\theta_2) = -\frac{2}{\sqrt{6}}\sin(\alpha). \tag{2}$$

$\alpha = 0$ corresponds to an orientation of $\vec{B}$ along the [011] direction. In the following, we compare the results to the more complicated case of a $\langle 111\rangle$-oriented wafer [cf. Fig. 2(a)]. Then, up to four frequency components are expected to contribute to the Larmor precession, one of which is constant [$\cos(\theta_1) = 0$]. The remaining θ_i are characterized by

$$\begin{aligned}\cos(\theta_2) &= \frac{2}{\sqrt{6}}\cos(\alpha) - \frac{2}{3\sqrt{2}}\sin(\alpha),\\ \cos(\theta_3) &= \frac{4}{3\sqrt{2}}\sin(\alpha),\\ \cos(\theta_4) &= \frac{2}{\sqrt{6}}\cos(\alpha) + \frac{2}{3\sqrt{2}}\sin(\alpha).\end{aligned} \tag{3}$$

Here α is measured relative to $[1\bar{1}0]$.

Figures 3 and 4 summarize a FFT analysis of the time-domain results for the samples A1 and B, respectively. While data points indicate the contributing frequency components g_i (the error bars specify the full width at half-maximum of the respective FFT peaks), the lines originate from fits to the model according to Eqs. (1), (2), and (3). The best overall agreement in sample A1 (B) is achieved with tensor elements of $g_l = 0.81 \pm 0.03$ and $g_t = 1.90 \pm 0.02$ ($g_l = 0.83 \pm 0.01$, $g_t = 1.90 \pm 0.01$). A similar analysis of the more strongly doped sample A2 (data not shown) reveals comparable values of $g_l = 0.77 \pm 0.03$ and $g_t = 1.91 \pm 0.02$. Taken together, the results consistently manifest the tensor character of $\mathbf{g}^*$ for L-valley electrons in bulk Ge. They are in good agreement with results from spin resonance on donor bound electrons in strained Sb-doped Ge (cf. $g_l = 0.828 \pm 0.003$ and $g_t = 1.915 \pm 0.001$ in Ref. 11 and references therein).

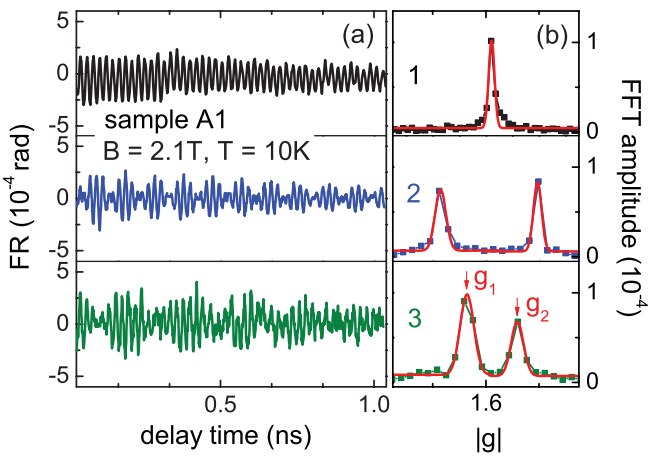

FIG. 1. (Color online) Electron spin coherence in sample A1 for different in-plane orientations of the magnetic field at $T = 10$ K and $B = 2.1$ T. (a) FR transients. (b) FFTs of the time-domain data. Lines: Gaussian fits to the FFT data to reveal the peak positions g_i. The numbers 1, 2, and 3 correspond to $\alpha = 45°$, $118°$, and $140°$ in the notation of Fig. 3.

III. RESULTS ON ELECTRON SPIN DECOHERENCE

We now turn to the decay of the electron spin coherence, which depends markedly on temperature, doping concentration, and the orientation of the magnetic field. To extract the coherence time τ, FR transients recorded at $B = 0.7$ T are fitted according to

$$\mathrm{FR}(t) = \sum_i A_i \exp(-t/\tau)\cos[(\omega_L)_i t], \tag{4}$$

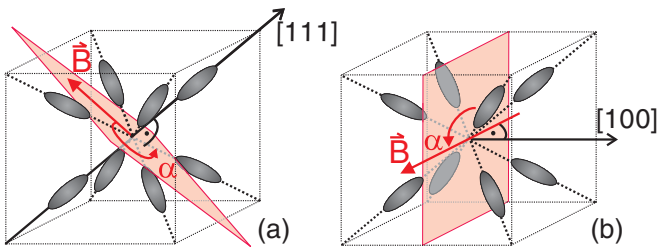

FIG. 2. (Color online) Surfaces of constant energy in Ge. The orientation of the in-plane magnetic field $\vec{B}$ is indicated for (a) sample B and (b) samples A1 and A2.

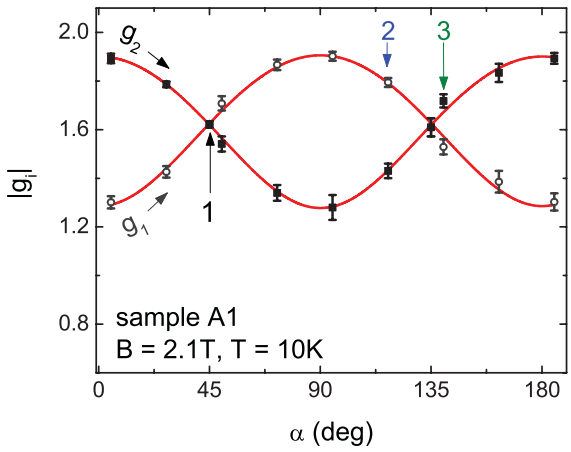

FIG. 3. (Color online) g anisotropy for sample A1. The components g_1 and g_2 are extracted from FR transients at $B = 2.1$ T and $T = 10$ K. The lines arise from Eq. (1) with $g_l = 0.81$ and $g_t = 1.90$. The numbered data points correspond to the transients in Fig. 1.

where A_i denote the initial amplitudes of the Larmor frequency components $(\omega_L)_i$. We assume a universal decoherence time for the components since this is found to be sufficient to achieve good agreement with the FR transients.

Figure 5 depicts τ as obtained for samples A1 (squares), A2 (circles), and B (triangles) at temperatures up to 200 K. We have chosen orientations of $\alpha = 45^\circ$ (60°) for samples A1 and A2 (sample B) so that only one (two) Larmor frequencies are present. Overall, τ varies from ~100 ps up to ~10 ns. The longest decay times seen for sample A1 at low temperatures provide a lower limit rather than an exact measure. This is related to a limited delay line of 3.7 ns. In addition, the model below points to a strong reduction of the apparent τ by minute misalignments of α.

From the data in Fig. 5, we assess four major characteristics: (i) Coherence times are practically constant below $T \sim 60$ K. (ii) A comparison of the ⟨100⟩-oriented samples A1 and A2

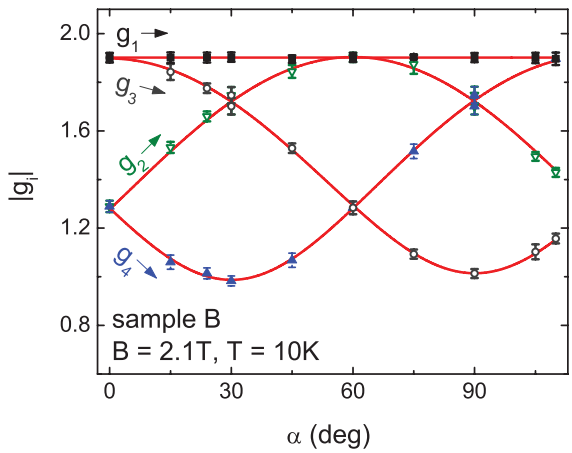

FIG. 4. (Color online) g anisotropy for sample B. The four frequency components g_i are extracted from FR transients at $B = 2.1$ T and $T = 10$ K. The lines are theoretical results according to Eq. (1) with $g_l = 0.83$ and $g_t = 1.90$.

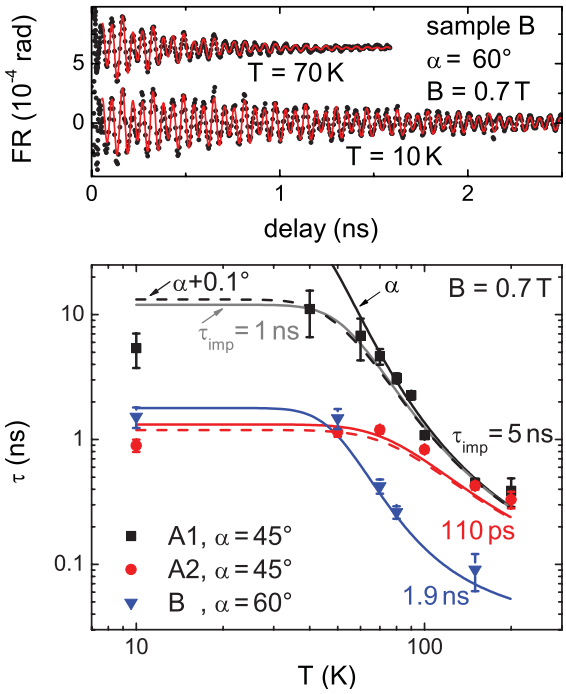

FIG. 5. (Color online) (a) Circles: Exemplary FR transients in sample B at $B = 0.7$ T and $\alpha = 60^\circ$. The lines are fits according to Eq. (4) to extract τ. (b) Temperature dependence of τ for samples A1 (squares), A2 (circles), and B (triangles) at $B = 0.7$ T. The solid lines show results of Eq. (5) for the indicated angles, while the dashed lines are for an angular deviation of 0.1°.

at low temperatures points to faster decoherence for stronger doping. (iii) At elevated temperatures $T > 60$ K, τ decreases while the influence of doping becomes less pronounced. (iv) Over the whole temperature range, τ is shorter for the ⟨111⟩-oriented sample B when compared to the similarly doped ⟨100⟩ specimen A1. The findings (i), (ii), and (iii) are consistent with Elliott-Yafet spin relaxation: due to spin-orbit mixing of the electron wave function, momentum scattering has a finite probability of a simultaneous spin flip.[13,14] This mechanism is expected to be dominant for conduction-band electrons in bulk Ge, especially since any D'yakonov-Perel process is forbidden in the inversion symmetric Ge lattice.[15] In principle, a spin flip can occur for both intra- and intervalley scattering. However, in a multivalley conduction band, momentum relaxation is dominated by intervalley processes.[16] While the unpronounced temperature dependence below 60 K indicates dominant impurity scattering, the decrease of τ beyond 60 K is in line with phonon-mediated spin relaxation. Aspect (iv) can be understood by considering scattering from a valley with an initial effective g factor g_i to a final state characterized by a different g_f. As is evident from Fig. 4, such processes are expected to occur in sample B for any angle α. After such a scattering event, the spin state of the electron dephases relative to the spins in both the initial and the final valley. The impact of scattering events with $\Delta g = |g_f - g_i| \neq 0$ on electron spin coherence is also expected in the ⟨100⟩-oriented samples away from $\alpha = 45^\circ$. To verify this, data for the angular dependence of τ in sample A2 are shown in Fig. 6.

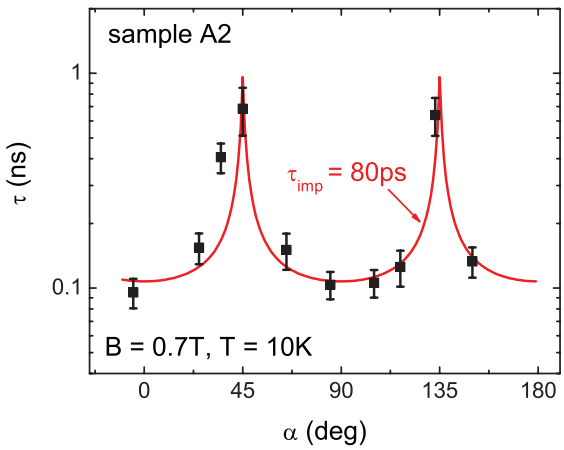

FIG. 6. (Color online) Influence of magnetic-field orientation on τ for sample A2. Squares: decay times extracted from FR transients in $B = 0.7$ T at $T = 10$ K. The line is the theoretical prediction according to Eq. (5) with $\tau_{imp} = 80$ ps.

They reveal a marked reduction of the coherence time τ for configurations of different g_1 and g_2 (cf. Fig. 3). In particular, the longest coherence is found for $\alpha = 45^\circ$ and 135°, where only one frequency component contributes to the signal and, consequently, intervalley scattering never changes g. In the undoped sample A1, similar trends are found: the decay time varies from > 5 ns for $\alpha = 45^\circ$ to 1 ns for $\alpha = 0^\circ$. In contrast, for sample B we find only a minor angular dependence of τ, because for every α valleys of different g are present (data not shown).

The qualitative analysis done so far indicates that a theoretical modeling of electron spin decoherence has to include impurity- as well as phonon-mediated intervalley scattering with either $\Delta g = 0$ or $\Delta g \neq 0$. For scattering processes into equivalent valleys ($\Delta g = 0$), we assume an intervalley scattering time of τ_{inter} and a probability c_{loss}^{-1} of a spin flip per scattering event. As a result, the decoherence rate for such processes is $\tau_{loss} = c_{loss} \times \tau_{inter}/2$. The factor of 2 accounts for the negative contribution of a flipped spin to the signal. For scattering with $\Delta g \neq 0$, a particular spin acquires a phase difference of $\pi/2$ relative to the remaining ensemble within $\tau_L = \frac{\pi/2}{(\Delta g \mu_B B)/\hbar}$ after the scattering event. Consequently, an estimate for the related decoherence time is $\tau_{decoh} = \tau_{inter} + \tau_L$. Note that this model for decoherence requires both a scattering process and some time of precession with an altered g factor so that decoherence is characterized by the slower of the two time constants. Assuming these decoherence channels to be independent, our model therefore suggests an overall decoherence time τ with

$$\tau^{-1} = \tau_{decoh}^{-1} + \tau_{loss}^{-1}. \quad (5)$$

τ shows an angular dependence since τ_L—and thus τ_{decoh}—is determined by Δg, which in turn depends on the orientation of the magnetic field (cf. Figs. 3 and 4). We model intervalley scattering as being composed of impurity- and phonon-mediated processes according to $\tau_{inter}^{-1} = \tau_{imp}^{-1} + \tau_{phon}^{-1}$. τ_{imp} is assumed to be independent of temperature. In contrast, the temperature dependence of the phonon contribution is[17]

TABLE II. Intervalley scattering times τ_{imp} for impurity-mediated processes. c_{loss}^{-1} is the probability of spin loss per intervalley scattering event. Parameters are deduced from best fits to the data in Figs. 5 and 6.

Sample	A1	A2	B
τ_{imp}	(5 ± 3) ns	(110 ± 50) ps	(1.9 ± 0.7) ns
c_{loss}		14–27	

$\tau_{phon} = 1/(2w_2)\exp(\Theta/T)$ with $w_2 = 10^{11\pm0.3}$ s^{-1} and $\theta = 315$ K $\pm$ 10% as extracted in Ref. 17 from experimental data for As-doped Ge.

Table II summarizes the values for τ_{imp} and c_{loss} and their possible ranges needed to well reproduce the data in Figs. 5 and 6. The parameter c_{loss} corresponds to a probability $c_{loss}^{-1} = 4\%-7\%$ for a spin flip per intervalley scattering event. While this value is larger than previous findings in highly doped material,[18] we note that additional decoherence channels inherent to the optically induced electron population might play a role, such as scattering within one valley or electron-hole scattering. For the extraction of τ_{imp}, one has to consider that minor misalignments of $\vec{B}$ may markedly reduce τ, especially for samples A1 and A2 in the vicinity of $\alpha = 45^\circ$ and 135°, where τ_L diverges. Model traces for perfect alignment are depicted as solid lines in Fig. 5: for sample A1, the trace with $\tau_{imp} = 1$ ns matches the data over the entire temperature range. In contrast, the curve with $\tau_{imp} = 5$ ns agrees well only at elevated temperatures but predicts $\tau \sim 60$ ns for low T. However, a curve with an experimentally inevitable $\Delta\alpha = 0.1^\circ$ (dashed lines) also agrees well with the experimental findings for $\tau(T)$. For sample A2, we find much shorter τ_{imp} as expected from stronger doping. In particular, the angular dependence of τ (cf. Fig. 6) is matched best with $\tau_{imp} = 80$ ps while a fit to the $\tau(T)$ points to a slightly larger value of $\tau_{imp} = 110$ ps (cf. Fig. 5). Such a drop of τ_{imp} upon lowering T is not included in our simplified model but is consistent with results in Ref. 17. The time scales are in line with predictions for impurity-mediated intervalley scattering times of $\sim$6 ns ($\sim$50 ps) for a 10^{14} cm^{-3} (5×10^{16} cm^{-3}) concentration of Sb donors in Ge at $T = 40$ K.[19] Taken together, our model explains the main dependences of τ on temperature, doping concentration, and magnetic-field orientation with reasonable parameters for intervalley scattering. Nevertheless, a detailed theoretical picture has to be developed to correctly address all possible scattering channels.

In conclusion, we have determined the effective Landé tensor $\mathbf{g}^*$ for photoinduced L-valley electrons in bulk Ge via ultrafast magneto-optics. The independent tensor elements are $g_t = 1.9$ and $g_l = 0.8$, in fair agreement with previous spin resonance results for donor-bound electrons. Electron spin decoherence occurs within $\sim$100 ps to $\sim$10 ns depending on temperature, doping concentration, and orientation of the external magnetic field with respect to the L-valley ellipsoids of constant energy. The characteristics of the decay time are explained in a basic model, taking into account a spin-flip probability of 4%–7% associated with intervalley scattering as well as decoherence due to scattering between valleys of different effective Landé factor.

ACKNOWLEDGMENTS

We wish to acknowledge support by and insightful discussions with N. Sircar, D. Bougeard, H. Huebl, M. Brandt, E. Sternemann, I. Akimov, D. Yakovlev, and M. Bayer. Initial work has been supported by the Sonderforschungsbereich SFB631 of the DFG.

*christine.hautmann@tu-dortmund.de

[1] I. Žutić, J. Fabian, and S. Das Sarma, Phys. Mod. Phys. **76**, 323 (2004).

[2] G. Lampel, Phys. Rev. Lett. **20**, 491 (1968).

[3] B. T. Jonker, G. Kioseoglou, A. T. Hanbicki, C. H. Li, and P. E. Thompson, Nat. Phys. **3**, 542 (2007).

[4] L. Grenet, M. Jarnet, P. Noé, V. Calvo, J.-M. Hartmann, L. E. Nistor, B. Rodmacq, S. Auffret, P. Warin, and Y. Samson, Appl. Phys. Lett. **94**, 032502 (2009).

[5] F. Roux, G. Lampel, Y. Lassailly, and J. Peretti, Bull. Am. Phys. Soc. **20**, 12 (2006).

[6] P. Li and H. Dery, Phys. Rev. Lett. **105**, 037204 (2010).

[7] C. Guite and V. Venkataraman, Phys. Rev. Lett. **107**, 166603 (2011).

[8] E. J. Loren, J. Rioux, C. Lange, J. E. Sipe, H. M. van Driel, and A. L. Smirl, Phys. Rev. B **84**, 214307 (2011).

[9] C. Hautmann, B. Surrer, and M. Betz, Phys. Rev. B **83**, 161203(R) (2011). Note that the values stated there for the hole and electron Landé factors are ∼4% too low due to a systematic error in the magnetic-field magnitude.

[10] L. M. Roth, Phys. Rev. **118**, 1534 (1960).

[11] E. B. Hale, J. R. Dennis, and S.-H. Pan, Phys. Rev. B **12**, 2553 (1975).

[12] L. M. Roth and B. Lax, Phys. Rev. Lett. **3**, 217 (1959).

[13] R. J. Elliott, Phys. Rev. **96**, 266 (1954).

[14] Y. Yafet, Solid State Phys. **14**, 1 (1963).

[15] M. I. D'yakonov and V. I. Perel', Fiz. Tverd. Tel. **13**, 3581 (1971) [Sov. Phys. Solid State **13**, 3023 (1972)].

[16] P. Y. Yu and M. Cardona, *Fundamentals of Semiconductors: Physics and Materials Properties*, Graduate Texts in Physics, 4th ed. (Springer-Verlag Berlin, Heidelberg, 2010).

[17] G. Weinreich, T. M. Sanders, and H. G. White, Phys. Rev. **114**, 33 (1959).

[18] J.-N. Chazalviel, J. Phys. Chem. Solids **36**, 387 (1975).

[19] W. P. Mason and T. B. Bateman, Phys. Rev. **134**, A1387 (1964).